

Time Crystal in a Single-mode Nonlinear Cavity

Yaohua Li¹, Chenyang Wang¹, Yuanjiang Tang¹, and Yong-Chun Liu^{1,2,*}

¹*State Key Laboratory of Low-Dimensional Quantum Physics,*

Department of Physics, Tsinghua University, Beijing 100084, P. R. China and

²*Frontier Science Center for Quantum Information, Beijing 100084, China*

(Dated: October 10, 2023)

Time crystal is a class of non-equilibrium phase with broken time-translational symmetry. Here we demonstrate the time crystal in a single-mode nonlinear cavity. The time crystal originates from the self-oscillation induced by the linear gain and is stabilized by the nonlinear damping. We show this time crystal model exhibits four different characteristics: the emergence of classical limit cycle under the mean-field approximation, the dissipative gap closing in the thermodynamic limit, the quantum oscillation in the Husimi function, and the emergence of quantum limit cycle in the steady state. These properties provide a complete description of the time crystal and thus pave the way to investigate the time crystal in nonlinear systems.

The concept of time crystal was first proposed by Shapere and Wilczek [1–4]. The time crystal is an analogy of the spacial crystal, and it is defined as a phase of matter where the time-translational symmetry of the ground state is spontaneously broken. However, the initially proposed model with spontaneously rotating ground state is ruled out by no-go theorems in subsequent studies [5–7]. The no-go theorems still allow closed systems with long-range couplings to break the time-translational symmetry, as verified in a spin-1/2 many-body Hamiltonian [8]. However, this model is also in dispute [9, 10]. The concept of time crystal is also generalized into periodically driven systems, as known as the discrete time crystal [11–18]. It is characterized by subharmonic oscillations and thus breaks the discrete time-translational symmetry. The discrete time crystal has already been realized in trapped ions [19, 20], nuclear spins [21–25] and other systems [26–31].

Introducing couplings to the environment is another method to circumvent the no-go theorem and to obtain time crystal dynamics [32–36]. This method can still start from a time-independent Hamiltonian and break the continuous time-translational symmetry [37–39]. Specifically, nonlinear systems with limit cycles are shown to be powerful platforms to realize this kind of time crystal [40, 41]. In classical systems, two essential conditions are proposed to distinguish a time crystal from normal limit cycle models: the oscillating phase takes random values from 0 to 2π for repeated realizations; the oscillation dynamics is robust against perturbations or fluctuations [42]. In quantum systems, the time crystal can be directly characterized by pure imaginary eigenvalues of Liouvillian spectrum in the thermodynamic limit [43–46]. However, it is still difficult to obtain a full quantum description of the time crystal in open and nonlinear systems, as these systems contain both many-body interactions and couplings to the environment.

Here we demonstrate that the time crystal can be realized in a single-mode nonlinear cavity. It can be exactly solved for large Fock space dimensions. Surprisingly, we

show such a simple model is enough to reveal the rich properties of a time crystal. In our model, the time crystal originates from the self-oscillation induced by the linear gain and is stabilized by the nonlinear damping. We show this time crystal model exhibits four different characteristics: the emergence of classical limit cycle under the mean-field approximation, the dissipative gap closing in the thermodynamic limit, the quantum oscillation exhibited in the Husimi function, and the emergence of quantum limit cycle in the steady state. These results pave a new promising way for further experiments and deepen our understanding of time crystals.

We consider a single-mode cavity described by the master equation ($\hbar = 1$):

$$\dot{\rho} = i[\rho, H] + \kappa \mathcal{D}[a]\rho + g\mathcal{D}[a^\dagger]\rho + \eta\mathcal{D}[a^2]\rho, \quad (1)$$

where ρ is the density matrix, a (a^\dagger) is the bosonic annihilation (creation) operator, and $\mathcal{D}(o)\rho = o\rho o^\dagger - (o^\dagger o\rho + \rho o^\dagger o)/2$ is the Liouvillian for operator o . We have standard terms for linear (single-photon) damping, linear gain, and nonlinear (two-photon) damping [47] with rates

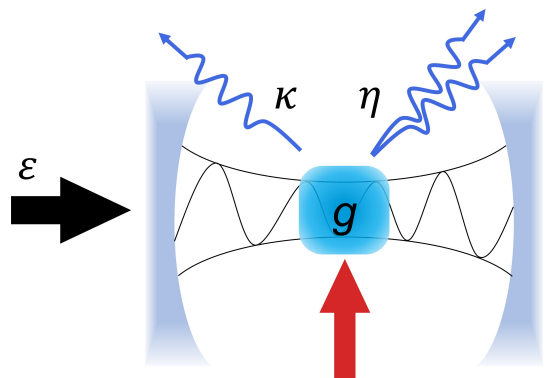


FIG. 1. Schematic representation of our setup: a cavity mode a under driving with strength ϵ . There are both linear (single-photon) and nonlinear (two-photon) damping with rates κ and η , respectively. There is also a linear gain with rate g , see Eq. (1).

κ , g and η , respectively [see Fig. 1]. The Hamiltonian with driving is $H = -\Delta a^\dagger a + \varepsilon a^\dagger + \varepsilon^* a$, where Δ is the detuning between the driving frequency and the cavity frequency, and ε is the strength of the driving protocol.

This model can be reduced to a driven Van der Pol oscillator under the mean-field approximation [48], where the evolution of amplitude $\alpha = \langle a \rangle$ is appropriately governed by

$$\dot{\alpha} = \left(-\frac{\kappa - g}{2} + i\Delta \right) \alpha - \eta |\alpha|^2 \alpha - i\varepsilon. \quad (2)$$

It is a famous model that has Hopf bifurcation and limit cycle phase. The Hopf bifurcation point, characterized by the modulated driving strength $\varepsilon\sqrt{\eta}$, is a constant, as Eq. (2) is the same after the transformation $\alpha \rightarrow \alpha\sqrt{N}$, $\varepsilon \rightarrow \varepsilon\sqrt{N}$ and $\eta \rightarrow \eta/N$, where N is a dimensionless parameter. This constant can be approximately obtained by letting $\eta \rightarrow 0$, which is

$$\varepsilon\sqrt{\eta} \approx \frac{\sqrt{(g - \kappa)[(g - \kappa)^2 + 4\Delta^2]}}{4}. \quad (3)$$

The dashed black line in Fig. 2(a) represents the Hopf bifurcation, and the pink (blue) area denotes the limit cycle (equilibrium) phase of the reduced classical model.

Beyond the well-established classical model, we are more interested in the non-equilibrium behavior at the full quantum level. We numerically solve the Liouvillian spectrum and the time evolution of the cavity mode in a truncated Fock basis with dimensions of 100. From the Liouvillian spectrum, we define a concept of “dissipative gap” Δ_λ as the largest real part of the eigenvalues with a nonzero imaginary part. This definition is a little different from that in Ref. [45], and can better characterize the dissipative properties in the non-equilibrium phase. Because a zero dissipative gap means the existence of pure imaginary eigenvalues.

In Fig. 2(a), we show the dissipative gap as a function of the modulated driving strength $\varepsilon\sqrt{\eta}$ for different nonlinear damping rate η . There is a rapid closing of the dissipative gap in the limit cycle phase when the nonlinear damping rate η approaches zero, i.e., the thermodynamic limit or the weak interaction limit. It indicates a kind of dissipative phase transition in the thermodynamic limit [49, 50]. Similar results have also been obtained in two-mode cavities [45]. However, due to the much larger dimensions of truncated Hilbert space that we can use, we obtain a much smoother dissipative gap-closing pattern, where the dissipative phase transition matches well with the Hopf bifurcation.

Importantly, the closing dissipative gap indicates a long-time quantum oscillation and also the emergence of the time crystal. It originates from the self-oscillation induced by the linear gain and is stabilized by the nonlinear damping, similar to the mechanism of the limit cycle emerging in the classical limit. At the quantum

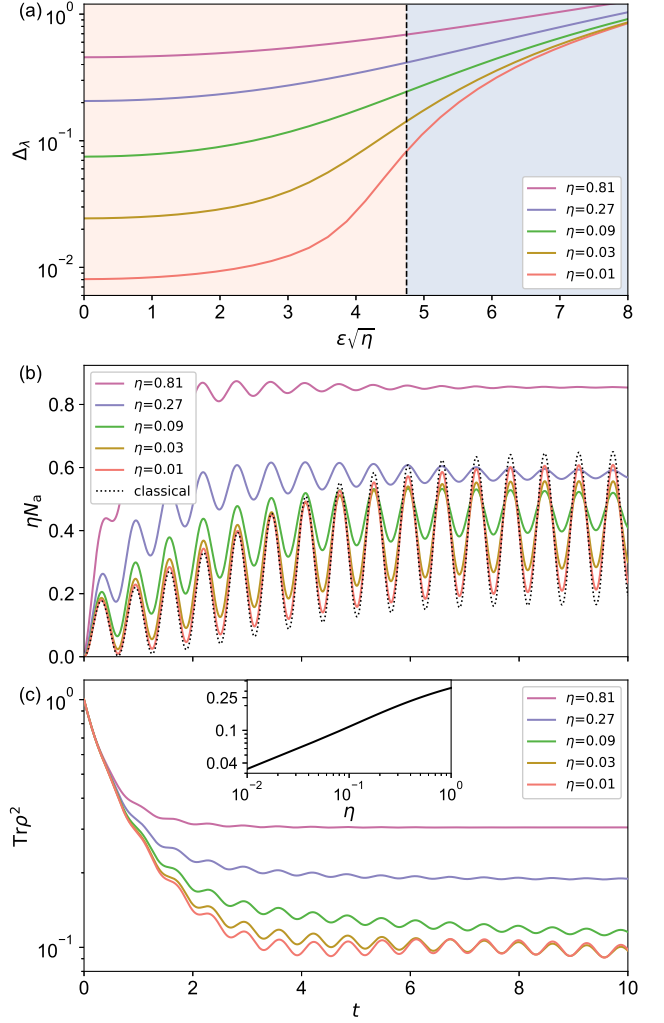


FIG. 2. Dissipative gap closing and stable quantum oscillation. (a) The dissipative gap as a function of modulated driving strength $\varepsilon\sqrt{\eta}$ for different nonlinear damping rate η . The black dashed line indicates the Hopf bifurcation of the reduced classical model, and the pink (blue) area indicates the limit cycle (equilibrium) phase. (b),(c) The time evolution of modulated photon number ηN_a (b) and state purity $\text{Tr}\rho^2$ (c). The black dashed line in (b) indicates the time evolution of the classical model. The inset shows the steady-state purity as a function of the nonlinear damping rate. The initial state is the vacuum state, and the modulated driving strength is chosen as $\varepsilon\sqrt{\eta} = 2$. Other parameters are $\Delta = 10$, $\kappa = 0.1$, and $g = 1$.

level, the real part of the Liouvillian spectrum is always non-positive, and there is always a steady state which satisfies $\mathcal{L}\rho_0 = 0$ (\mathcal{L} is the total Liouvillian superoperator in the master equation). However, the time arriving at the steady state becomes infinite when the dissipative gap closes in the thermodynamic limit. Consequently, we also denote the limit cycle phase as the time crystal phase in the following.

To capture the non-equilibrium oscillating behavior at

the quantum level, we compute the time evolution of photon number $N_a = \langle a^\dagger a \rangle$ for four different values of nonlinear damping rate η , as shown in Fig. 2(b). The initial state is a vacuum state, and the modulated driving strength is all chosen as $\varepsilon\sqrt{\eta} = 2$. The vertical value is modulated photon number (the photon number multiplied by the nonlinear damping rate ηN_a) to eliminate the amplitude amplification for small nonlinear damping rates. We also plot the classical time evolution governed by Eq. (2) starting from $\alpha = 0$ (black dashed line). As we reduce the nonlinear damping rate, a stable quantum oscillation emerges with both increasing oscillation amplitude and increasing relaxation time. This oscillating behavior verifies the closing dissipative gap in the thermodynamic limit and thus proves itself a time crystal. When the nonlinear damping rate approaches zero, the time evolution at the quantum level approaches the classical time evolution.

The quantum-classical transition is more clear when we look at the state purity $\text{Tr}\rho^2$. The inset in Fig. 2(c) shows the steady-state purity as a function of the nonlinear damping rate. The state purity approaches zero with a fixed scaling when we decrease the nonlinear damping rate. For smaller nonlinear damping rates, the driving strength is enlarged as $\varepsilon\sqrt{\eta}$ remains fixed. In this case, the steady state is driven into a higher-occupation state in the Fock space and more Fock basises are included. Consequently, the steady state is more like a classical equilibrium state in the thermodynamic limit.

In Fig. 2(c), we also plot the time evolution of state purity, which contains rich phenomena that have not been found in other time crystal models before. The initial state is the vacuum state with purity $\text{Tr}\rho^2 = 1$. In the beginning, the state purity decreases quickly with a similar rate for different nonlinear damping rates. The decreasing processes continue for longer times when the nonlinear damping rate is smaller, resulting in a smaller final state purity after the long-time evolution. After the quick decrease, the system enters an oscillating regime before the final relaxation to the steady state. It is a metastability regime, originating from a large separation between two consecutive eigenvalues [51]. Moreover, the state purity is partially preserved in the metastability regime. Looking at the bottom two lines in Fig. 2(c) ($\eta = 0.03$ and 0.01), the state purity does not decrease when we further reduce the nonlinear damping rate, which is distinct from the behavior of the steady-state purity. It reveals that this time crystal phase can partially preserve the information in the initial state and may find application in quantum associative memory [51].

Next, we investigate the quantum oscillation from a quasiprobability distribution, i.e., the Husimi Q-function defined as $Q_q(\alpha) = \langle \alpha | \rho | \alpha \rangle$. The subscript q denotes it is a quantum distribution function, as we also consider the classical probability distribution $Q_c(\alpha)$. Figure 3(a) shows snapshots of the Husimi distribution around an os-

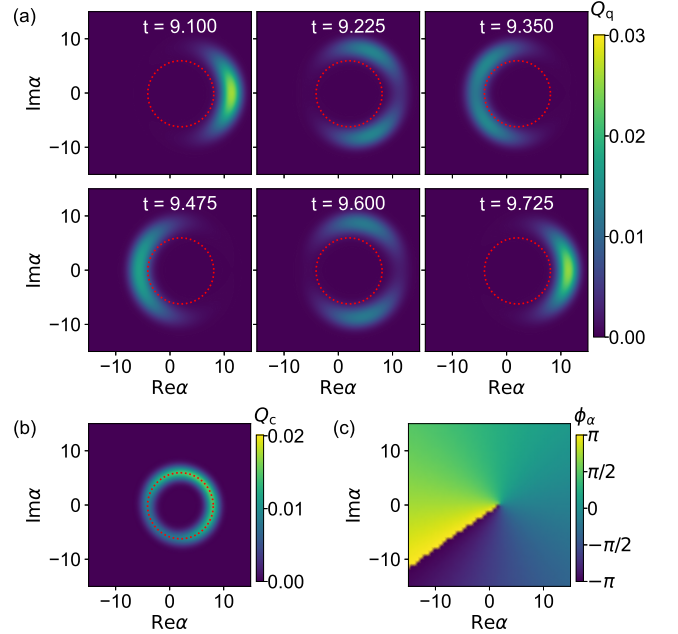


FIG. 3. The quantum and classical Husimi distributions. (a) Snapshots of the quantum Husimi distribution around an oscillating period. (b) Classical Husimi distribution at $t = 10$. The initial states are both the vacuum state. (c) Oscillating phases in the classical trajectory at $t = 10$. The oscillating phase depends on the start point in the phase space. There is a singular point where the oscillating phase is not continuous. The parameters are $\Delta = 10$, $\kappa = 0.1$, $g = 1$, $\eta = 0.01$, and $\varepsilon\sqrt{\eta} = 2$.

cillating period corresponding to an initial vacuum state [52]. Surprisingly, we find the evolution of the Husimi distribution is not a rotation but is swinging from left to right and backward. It is distinct from the classical evolution in a limit cycle. As a comparison, we also plot in Fig. 3(b) the classical probability distribution at $t = 10$. It is obtained through the Monte Carlo simulations with 10000 trajectories, where the initial distribution also uses the vacuum state. In the reduced classical model the probability distribution directly decays to fulfill the limit cycle and remains dispersed along the limit cycle. The red dashed lines in Fig. 3(a) and 3(b) denote the limit cycle. The oscillation emerges in every single trajectory but disappears in the probability distribution due to the dispersed oscillating phases. Differently, the quantum oscillation is encoded in the Husimi distributions and remains for a long time. The oscillating quantum Husimi distribution is a major finding of this work as a characteristic of the quantum time crystal beyond the classical limit cycle.

To determine the origin of the dispersed oscillating phases emerging in the classical trajectories, we show in Fig. 3(c) the oscillating phases at $t = 10$ versus the place of the initial state in the phase space. The oscillating

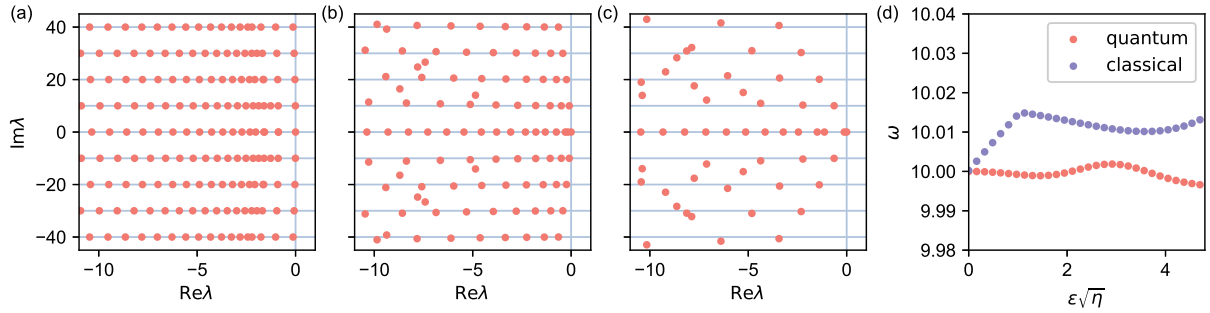


FIG. 4. Liouvillian spectra for $\varepsilon\sqrt{\eta} = 0$ (a), $\varepsilon\sqrt{\eta} = 4.8$ (b) and $\varepsilon\sqrt{\eta} = 7.2$ (c), corresponding to the time crystal phase, equilibrium phase and the critical phase between them. The red points are the eigenvalues, while the horizontal blue lines denote a frequency scale equal to the detuning Δ . (d) The oscillating frequencies as a function of the modulated driving strength. The quantum results (red points) are the imaginary part of the eigenvalues with the largest real part and nonzero imaginary part. The classical results (blue points) are obtained by solving the limit cycle through the Poincaré map. Other parameters are $\Delta = 10$, $\kappa = 0.1$, $g = 1$, and $\eta = 0.01$.

phase is continuous when the initial state changes in the phase space except for a singular point. Starting from this point, the oscillating phase is highly uncertain as an infinitely small error in the initial state can lead to any possible phase in the final limit cycle. The probability distribution in Fig. 3(b) is obtained with an initial probability distribution of the vacuum state, which covers the singular point and thus results in a dispersed probability distribution along the limit cycle. Moreover, the vacuum state is a two-dimensional Gaussian distribution centered in the origin while the singular point of the oscillating phase deviates from the origin. It results in the ununiform distribution of the oscillating phase in Fig. 3(b).

To provide further insight into the non-equilibrium dynamic of the quantum system, we compute the full Liouvillian spectra for three different parameters, corresponding to the time crystal phase [Fig. 4(a)], equilibrium phase [Fig. 4(c)] and the critical phase between them [Fig. 4(b)]. There is a global characteristic of the Liouvillian spectra. First, the Liouvillian spectra are always non-positive, and there is only one eigenvalue that is absolutely zero, corresponding to the final equilibrium state. Due to the property that the Liouvillian operator has zero trace, other eigenvectors of the Liouvillian operator in the matrix form indeed also have zero trace. Consequently, these eigenvectors do not correspond to any real density matrices (which have unit trace). It also means that these eigenvectors will contribute to the evolution starting from any initial state, which makes the quantum oscillation in the time crystal phase a strong breaking of ergodicity [53, 54].

From the spectra, we can find a frequency scale equal to the detuning Δ . The frequency scale is more clear for smaller driving strengths. Especially, when there is no driving, i.e., $\varepsilon = 0$, the elements in different diagonal lines of the density matrix are independent. The evolution of

elements in the m th diagonal line is governed by

$$\begin{aligned} \dot{p}_n = & -im\Delta p_n + \kappa \left[\sqrt{n(n+m)}p_{n-1} - \frac{2n+m}{2}p_n \right] \\ & + g \left[\sqrt{(n+1)(n+m+1)}p_{n+1} - \frac{2n+m+2}{2}p_n \right] \\ & + \eta \sqrt{n(n-1)(n+m)(n+m-1)}p_{n-2} \\ & - \eta \frac{n(n-1)+(n-m)(n-m-1)}{2}p_n, \end{aligned} \quad (4)$$

where $p_n = p_{n,n+m}$ denotes the n th element in the m th diagonal line, $m \in \mathbb{Z}$, and $n \geq \max(0, -m)$. In this case, the Liouvillian operator can be block diagonalized, and the imaginary part of the eigenvalues can be directly obtained as $-im\Delta$. It accounts for the equal spacing spectrum along the imaginary axis in Fig. 4(a). This property gradually disappears when we increase the driving strength. However, the right several eigenvalues with small real parts preserve the equal spacing frequency. It is also these eigenvalues that govern the non-equilibrium dynamics and thus the oscillating frequency remains similar to the detuning. As a comparison, the frequency of classical limit cycle is more dependent on the driving strength [see Fig. 4(d)].

A special case of our model (zero driving) has been investigated in Ref. [48], where they discover the quantum limit cycle in the steady state. Here we further show the emergence of quantum limit cycle is related to the time crystal phase and indicates a dissipative phase transition. As shown in Fig. 5(a), the quantum limit cycle emerges when we decrease the driving strength. The parameter region of quantum limit cycle agrees with the region of classical limit cycle and the region where the dissipative gap closes, and thus the quantum limit cycle can be regarded as another phenomenon related to the time crystal.

Furthermore, we show in Fig. 5(b) and 5(c) two steady-state observables as a function of the modulated

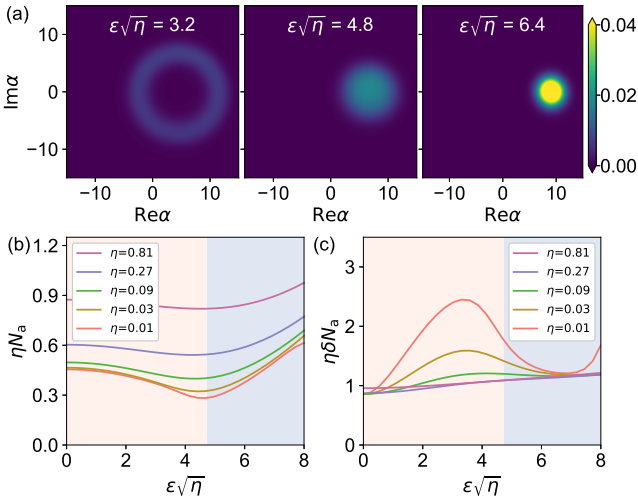


FIG. 5. Quantum limit cycle and observables in the steady state. (a) Steady-state quantum Husimi distributions for $\varepsilon\sqrt{\eta} = 3.2, 4.8, 6.4$ from left to right. The nonlinear damping rate is $\eta = 0.01$. (b),(c) The modulated photon number (b) and the modulated photon number fluctuation (c) for five different nonlinear damping rates η . Other parameters are $\Delta = 10$, $\kappa = 0.1$, and $g = 1$.

driving strength, i.e., the photon number and the photon number fluctuation. We also observe a sharp transition close to the phase boundary (Hopf bifurcation) in the thermodynamic limit. Interestingly, the average value and fluctuation of photon number, after eliminating the amplification by multiplied with a factor η , exhibit different behaviors. The modulated photon number ηN_a is suppressed especially at the phase boundary when increasing the nonlinear damping rate. In contrast, the modulated photon number fluctuation $\eta\delta N_a$ is strongly enhanced especially at the time crystal phase.

In conclusion, we investigate the non-equilibrium and equilibrium behaviors of the time crystal in a single-model nonlinear cavity. We show this time crystal model exhibits four different characteristics: the emergence of classical limit cycle under the mean-field approximation, the dissipative gap closing in the thermodynamic limit, the quantum oscillation exhibited in the Husimi function, and the emergence of quantum limit cycle in the steady state. Although several of these characteristics have been individually discovered in previous works, it is the first time to unify them together. Moreover, as the model we consider is the most simple classical model with limit cycles, our work reveals a fact that the time crystal may be a general quantum phenomenon in those systems that exhibit limit cycles under approximate classical description. Our results pave the way to investigate the time crystal in the quantum evolution of bosonic modes and may find application in quantum associative memory.

* ycliu@tsinghua.edu.cn

- [1] A. Shapere and F. Wilczek, Classical time crystals, *Phys. Rev. Lett.* **109**, 160402 (2012).
- [2] F. Wilczek, Quantum time crystals, *Phys. Rev. Lett.* **109**, 160401 (2012).
- [3] T. Li, Z.-X. Gong, Z.-Q. Yin, H. T. Quan, X. Yin, P. Zhang, L.-M. Duan, and X. Zhang, Space-time crystals of trapped ions, *Phys. Rev. Lett.* **109**, 163001 (2012).
- [4] F. Wilczek, Superfluidity and space-time translation symmetry breaking, *Phys. Rev. Lett.* **111**, 250402 (2013).
- [5] P. Bruno, Comment on “quantum time crystals”, *Phys. Rev. Lett.* **110**, 118901 (2013).
- [6] P. Bruno, Impossibility of spontaneously rotating time crystals: A no-go theorem, *Phys. Rev. Lett.* **111**, 070402 (2013).
- [7] H. Watanabe and M. Oshikawa, Absence of quantum time crystals, *Phys. Rev. Lett.* **114**, 251603 (2015).
- [8] V. K. Kozin and O. Kyriienko, Quantum time crystals from hamiltonians with long-range interactions, *Phys. Rev. Lett.* **123**, 210602 (2019).
- [9] V. Khemani, R. Moessner, and S. L. Sondhi, Comment on “Quantum Time Crystals from Hamiltonians with Long-Range Interactions”, [arXiv:2001.11037](https://arxiv.org/abs/2001.11037) .
- [10] V. K. Kozin and O. Kyriienko, Reply to “Comment on “Quantum Time Crystals from Hamiltonians with Long-Range Interactions””, [arXiv:2005.06321](https://arxiv.org/abs/2005.06321) .
- [11] M. P. Zaletel, M. Lukin, C. Monroe, C. Nayak, F. Wilczek, and N. Y. Yao, Colloquium: Quantum and classical discrete time crystals, *Rev. Mod. Phys.* **95**, 031001 (2023).
- [12] K. Sacha, Modeling spontaneous breaking of time-translation symmetry, *Phys. Rev. A* **91**, 033617 (2015).
- [13] D. V. Else, B. Bauer, and C. Nayak, Floquet time crystals, *Phys. Rev. Lett.* **117**, 090402 (2016).
- [14] N. Y. Yao, A. C. Potter, I.-D. Potirniche, and A. Vishwanath, Discrete time crystals: Rigidity, criticality, and realizations, *Phys. Rev. Lett.* **118**, 030401 (2017).
- [15] B. Huang, Y.-H. Wu, and W. V. Liu, Clean floquet time crystals: Models and realizations in cold atoms, *Phys. Rev. Lett.* **120**, 110603 (2018).
- [16] A. Pizzi, J. Knolle, and A. Nunnenkamp, Period- n discrete time crystals and quasicrystals with ultracold bosons, *Phys. Rev. Lett.* **123**, 150601 (2019).
- [17] N. Y. Yao, C. Nayak, L. Balents, and M. P. Zaletel, Classical discrete time crystals, *Nat. Phys.* **16**, 438 (2020).
- [18] S. Liu, S.-X. Zhang, C.-Y. Hsieh, S. Zhang, and H. Yao, Discrete time crystal enabled by stark many-body localization, *Phys. Rev. Lett.* **130**, 120403 (2023).
- [19] J. Zhang, P. W. Hess, A. Kyprianidis, P. Becker, A. Lee, J. Smith, G. Pagano, I.-D. Potirniche, A. C. Potter, A. Vishwanath, N. Y. Yao, and C. Monroe, Observation of a discrete time crystal, *Nature (London)* **543**, 217 (2017).
- [20] A. Kyprianidis, F. Machado, W. Morong, P. Becker, K. S. Collins, D. V. Else, L. Feng, P. W. Hess, C. Nayak, G. Pagano, N. Y. Yao, and C. Monroe, Observation of a prethermal discrete time crystal, *Science* **372**, 1192 (2021).
- [21] S. Choi, J. Choi, R. Landig, G. Kucsko, H. Zhou, J. Isoya, F. Jelezko, S. Onoda, H. Sumiya, V. Khe

mani, C. von Keyserlingk, N. Y. Yao, E. Demler, and M. D. Lukin, Observation of discrete time-crystalline order in a disordered dipolar many-body system, *Nature (London)* **543**, 221 (2017).

[22] J. Rovny, R. L. Blum, and S. E. Barrett, Observation of discrete-time-crystal signatures in an ordered dipolar many-body system, *Phys. Rev. Lett.* **120**, 180603 (2018).

[23] S. Pal, N. Nishad, T. S. Mahesh, and G. J. Sreejith, Temporal order in periodically driven spins in star-shaped clusters, *Phys. Rev. Lett.* **120**, 180602 (2018).

[24] J. O’Sullivan, O. Lunt, C. W. Zollitsch, M. L. W. Theuwalt, J. J. L. Morton, and A. Pal, Signatures of discrete time crystalline order in dissipative spin ensembles, *New J. Phys.* **22**, 085001 (2020).

[25] J. Randall, C. E. Bradley, F. V. van der Gronden, A. Galicia, M. H. Abobeih, M. Markham, D. J. Twitchen, F. Machado, N. Y. Yao, and T. H. Taminiau, Many-body-localized discrete time crystal with a programmable spin-based quantum simulator, *Science* **374**, 1474 (2021).

[26] J. Smits, L. Liao, H. T. C. Stoof, and P. van der Straten, Observation of a space-time crystal in a superfluid quantum gas, *Phys. Rev. Lett.* **121**, 185301 (2018).

[27] S. Autti, V. B. Eltsov, and G. E. Volovik, Observation of a time quasicrystal and its transition to a superfluid time crystal, *Phys. Rev. Lett.* **120**, 215301 (2018).

[28] C. Ying, Q. Guo, S. Li, M. Gong, X.-H. Deng, F. Chen, C. Zha, Y. Ye, C. Wang, Q. Zhu, S. Wang, Y. Zhao, H. Qian, S. Guo, Y. Wu, H. Rong, H. Deng, F. Liang, J. Lin, Y. Xu, C.-Z. Peng, C.-Y. Lu, Z.-Q. Yin, X. Zhu, and J.-W. Pan, Floquet prethermal phase protected by $u(1)$ symmetry on a superconducting quantum processor, *Phys. Rev. A* **105**, 012418 (2022).

[29] X. Mi, M. Ippoliti, C. Quintana, A. Greene, Z. Chen, J. Gross, F. Arute, K. Arya, J. Atalaya, R. Babbush, J. C. Bardin, J. Basso, A. Bengtsson, A. Bilmes, A. Bourassa, L. Brill, M. Broughton, B. B. Buckley, D. A. Buell, and B. Burkett *et al.*, Time-crystalline eigenstate order on a quantum processor, *Nature (London)* **601**, 531 (2022).

[30] X. Zhang, W. Jiang, J. Deng, K. Wang, J. Chen, P. Zhang, W. Ren, H. Dong, S. Xu, Y. Gao, F. Jin, X. Zhu, Q. Guo, H. Li, C. Song, A. V. Gorshkov, T. Iadecola, F. Liu, Z.-X. Gong, Z. Wang, D.-L. Deng, and H. Wang, Digital quantum simulation of Floquet symmetry-protected topological phases, *Nature (London)* **607**, 468 (2022).

[31] P. Frey and S. Rachel, Realization of a discrete time crystal on 57 qubits of a quantum computer, *Science Advances* **8**, eabm7652 (2022).

[32] Z. Gong, R. Hamazaki, and M. Ueda, Discrete time-crystalline order in cavity and circuit qed systems, *Phys. Rev. Lett.* **120**, 040404 (2018).

[33] H. Keßler, P. Kongkhambut, C. Georges, L. Mathey, J. G. Cosme, and A. Hemmerich, Observation of a dissipative time crystal, *Phys. Rev. Lett.* **127**, 043602 (2021).

[34] P. Kongkhambut, H. Keßler, J. Skulte, L. Mathey, J. G. Cosme, and A. Hemmerich, Realization of a periodically driven open three-level dicke model, *Phys. Rev. Lett.* **127**, 253601 (2021).

[35] H. Taheri, A. B. Matsko, L. Maleki, and K. Sacha, All-optical dissipative discrete time crystals, *Nat. Commun.* **13**, 848 (2022).

[36] M. Yue and Z. Cai, Prethermal time-crystalline spin ice and monopole confinement in a driven magnet, *Phys. Rev. Lett.* **131**, 056502 (2023).

[37] B. Buča, J. Tindall, and D. Jaksch, Non-stationary coherent quantum many-body dynamics through dissipation, *Nat. Commun.* **10**, 1730 (2019).

[38] M. Krishna, P. Solanki, M. Hajdušek, and S. Vinjanampathy, Measurement-induced continuous time crystals, *Phys. Rev. Lett.* **130**, 150401 (2023).

[39] L. d. S. Souza, L. F. dos Prazeres, and F. Iemini, Sufficient condition for gapless spin-boson lindbladians, and its connection to dissipative time crystals, *Phys. Rev. Lett.* **130**, 180401 (2023).

[40] H. Keßler, J. G. Cosme, M. Hemmerling, L. Mathey, and A. Hemmerich, Emergent limit cycles and time crystal dynamics in an atom-cavity system, *Phys. Rev. A* **99**, 053605 (2019).

[41] T. Liu, J.-Y. Ou, K. F. MacDonald, and N. I. Zheludev, Photonic metamaterial analogue of a continuous time crystal, *Nat. Phys.* **1** (2023).

[42] P. Kongkhambut, J. Skulte, L. Mathey, J. G. Cosme, A. Hemmerich, and H. Keßler, Observation of a continuous time crystal, *Science* **0**, eab03382 (2022).

[43] F. Iemini, A. Russomanno, J. Keeling, M. Schirò, M. Dalmonte, and R. Fazio, Boundary time crystals, *Phys. Rev. Lett.* **121**, 035301 (2018).

[44] K. Seibold, R. Rota, and V. Savona, Dissipative time crystal in an asymmetric nonlinear photonic dimer, *Phys. Rev. A* **101**, 033839 (2020).

[45] L. R. Bakker, M. S. Bahovadinov, D. V. Kurlov, V. Gritsev, A. K. Fedorov, and D. O. Krimer, Driven-Dissipative Time Crystalline Phases in a Two-Mode Bosonic System with Kerr Nonlinearity, *Phys. Rev. Lett.* **129**, 250401 (2022).

[46] Y. Nakanishi and T. Sasamoto, Dissipative time crystals originating from parity-time symmetry, *Phys. Rev. A* **107**, L010201 (2023).

[47] Z. Leghtas, S. Touzard, I. M. Pop, A. Kou, B. Vlastakis, A. Petrenko, K. M. Sliwa, A. Narla, S. Shankar, M. J. Hatridge, M. Reagor, L. Frunzio, R. J. Schoelkopf, M. Mirrahimi, and M. H. Devoret, Confining the state of light to a quantum manifold by engineered two-photon loss, *Science* **347**, 853 (2015).

[48] L. Ben Arosh, M. C. Cross, and R. Lifshitz, Quantum limit cycles and the Rayleigh and van der Pol oscillators, *Phys. Rev. Res.* **3**, 013130 (2021).

[49] E. M. Kessler, G. Giedke, A. Imamoglu, S. F. Yelin, M. D. Lukin, and J. I. Cirac, Dissipative phase transition in a central spin system, *Phys. Rev. A* **86**, 012116 (2012).

[50] M.-J. Hwang, P. Rabl, and M. B. Plenio, Dissipative phase transition in the open quantum rabi model, *Phys. Rev. A* **97**, 013825 (2018).

[51] A. Labay-Mora, R. Zambrini, and G. L. Giorgi, Quantum associative memory with a single driven-dissipative nonlinear oscillator, *Phys. Rev. Lett.* **130**, 190602 (2023).

[52] J. R. Johansson, P. D. Nation, and F. Nori, Qutip: An open-source python framework for the dynamics of open quantum systems, *Comp. Phys. Comm.* **183** (2012).

[53] C. J. Turner, A. A. Michailidis, D. A. Abanin, M. Serbyn, and Z. Papić, Weak ergodicity breaking from quantum many-body scars, *Nat. Phys.* **14**, 745 (2018).

[54] M. Schechter and T. Iadecola, Weak ergodicity breaking and quantum many-body scars in spin-1 XY magnets,

